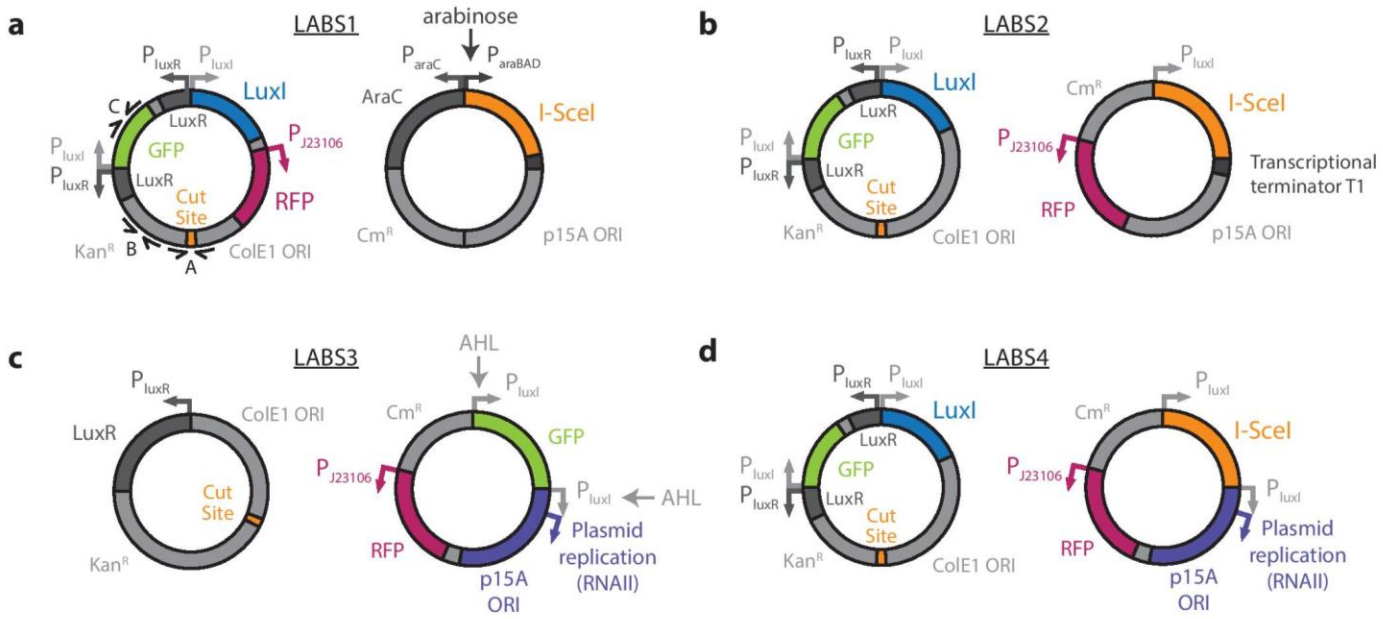

Supplementary Figure 1

Plasmid diagrams of primary strains used in this work.

Refer to Supplementary Table 1 for additional information and full list of strains. Diagrams are not to scale. (a) Strain used to demonstrate and quantify ColE1 copy number repression by I-SceI. A, B, and C refers to primer sets used for qPCR as shown in Supplementary Figure 2. (b) Plasmid copy number oscillator strain without RNAII overexpression. Note the transcriptional terminator downstream of *SCEI* preventing transcription from progressing into the p15A origin. (c) Strain used to visualize and quantify p15A copy number amplification by RNAII overproduction. The transcriptional terminator before the p15A origin has been replaced with a second copy of the *luxI* promoter, and the *SCEI* gene with a *gfp* gene. (d) Plasmid copy number oscillator strain modified to include RNAII overproduction under control of the *luxI* promoter as in LABS3.

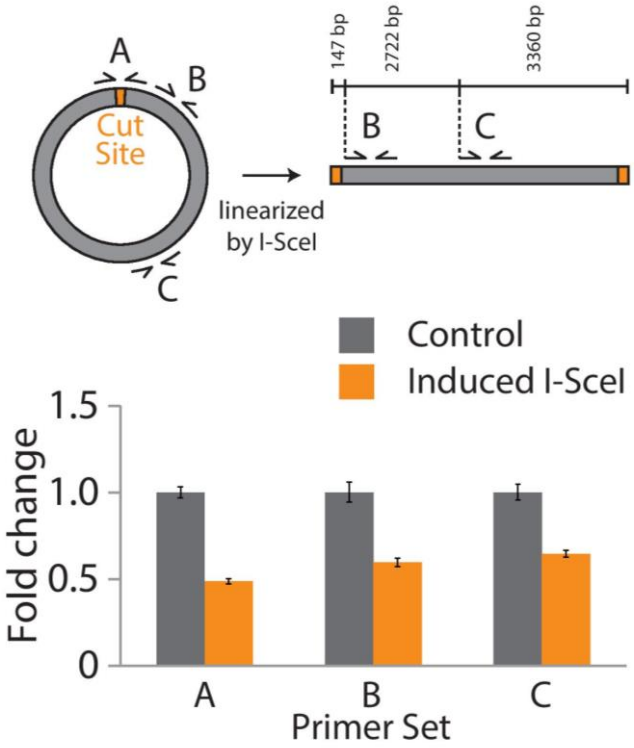

Supplementary Figure 2

qPCR analysis of ColE1 copy number repression.

qPCR analysis of ColE1 copy number repression after I-SceI induction with 0.2% w/v arabinose for 3 hours, using multiple primer sets annealing at different locations around the plasmid. Results demonstrate that after being cut by I-SceI, the majority of linear plasmids are quickly degraded. Primer set A is the same that used to quantify copy number in Figure 1, a. Mean and s.e.m. are displayed. Statistical significance was calculated by independent 2-sample *t* test with d.f. = 18, yielding $P = 6 \times 10^{-12}$ for primer set A, $P = 9 \times 10^{-7}$ for primer set B, and $P = 2 \times 10^{-7}$ for primer set C. See Methods for detailed description of experimental design, Supplementary Figure 1 for detailed plasmid diagrams, and Supplementary Table 2 for primer sequences.

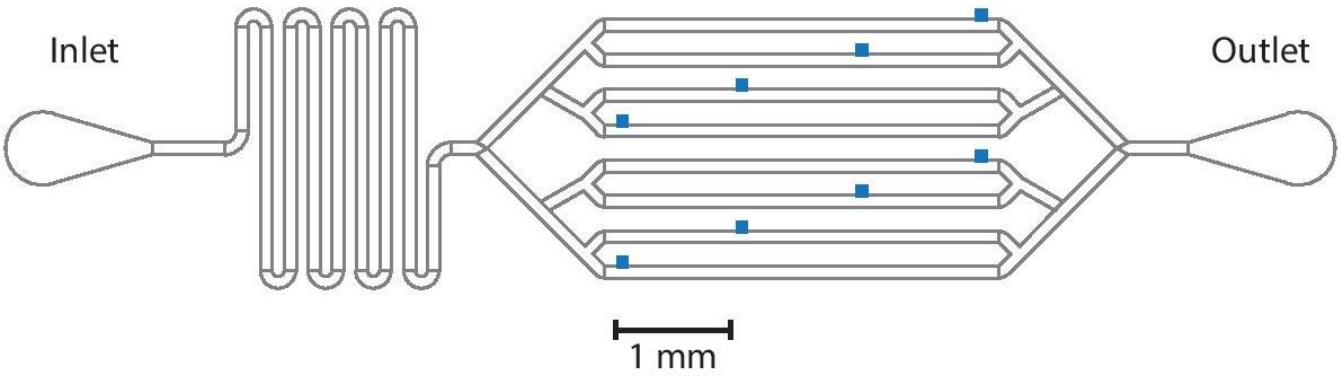

Supplementary Figure 3

Schematic of microfluidic device 1.

Each flow channel feeds growth medium to a single cell chamber (displayed in blue), preventing AHL diffusion between individual chambers. Flat rectangular chambers (x, y, z = 100 µm, 85 µm, 1.6 µm) allow visualization of single *E. coli* cells. Flow channels are 30 µm high.

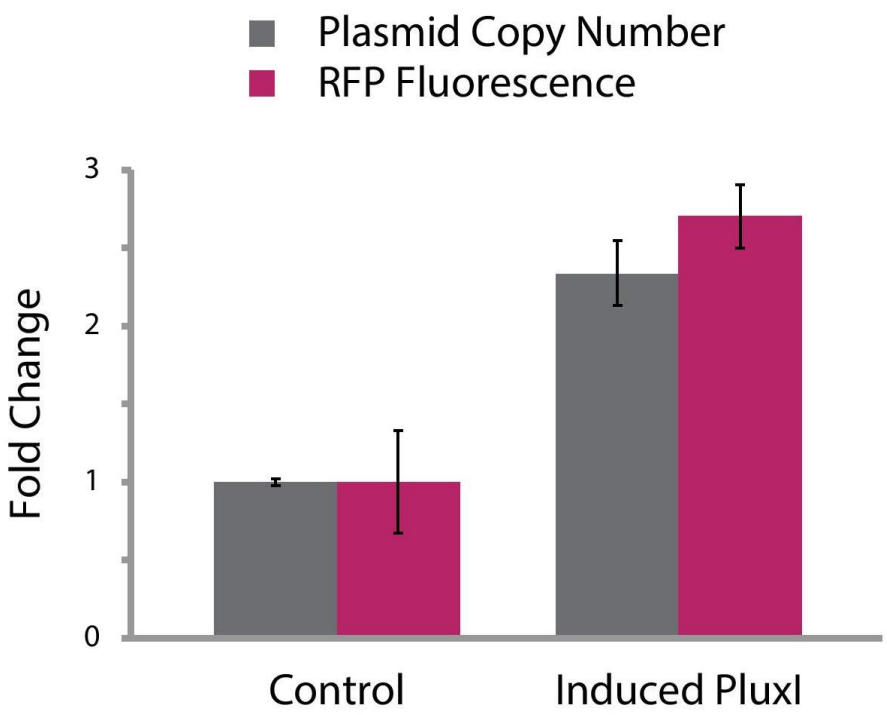

Supplementary Figure 4

qPCR analysis of p15A copy number amplification by RNAII overexpression.

Copy number amplification after 90 minutes of induction with 450 nM AHL, where PluxI promoter induction leads to RNAII overexpression from the p15A origin. Mean and s.e.m. are displayed. Statistical significance was calculated by independent 2-sample *t* test with d.f. = 18, yielding $P = 3 \times 10^{-8}$ for plasmid copy number and $P = 3 \times 10^{-4}$ for RFP fluorescence. See Methods for detailed description of experimental design, Supplementary Figure 1 for detailed plasmid diagrams, and Supplementary Table 2 for primer sequences.

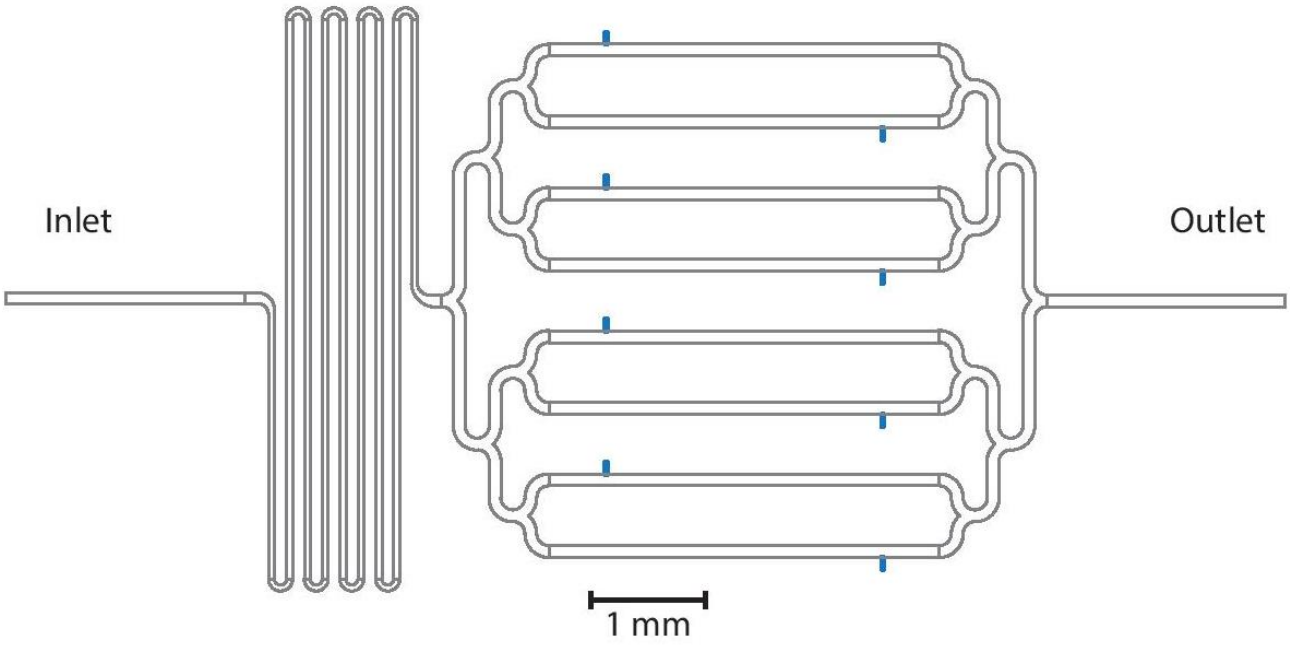

Supplementary Figure 5

Schematic of microfluidic device 2.

Each flow channel feeds growth medium to a single cell chamber (displayed in blue), preventing AHL diffusion between individual chambers. Larger and taller chambers (x, y, z = 15 µm, 100 µm, 50 µm) allow exploration of circuit dynamics in an alternate geometry. Flow channels are the same height as chambers at 50 µm.

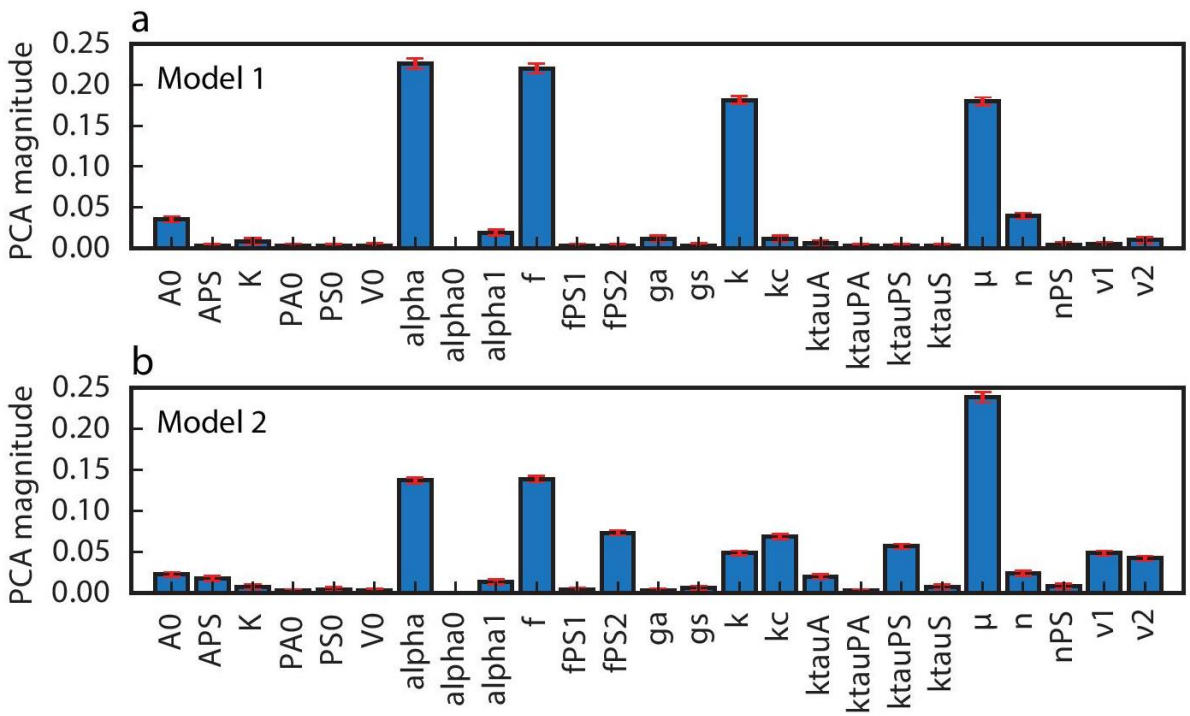

Supplementary Figure 6

PCA analysis of sensitive parameters.

Robustness analysis was done to identify which parameters most sensitively control oscillations (see Supplementary Note for details). For (a) model 1 and (b) model 2, we formed non-oscillatory parameter sets from the data used to generate Figure 3, e, and we determined the principal components with the lowest coefficient of variation (a proxy for sensitivity in this set). We examined representative non-oscillatory sets using $\eta = 0.3$ and $\eta = 0.1$ when studying model 1 and model 2, respectively, containing non-oscillatory parameter set sizes of 5,869 and 6,468, respectively. The principal component with the least coefficient of variation was found using standard techniques, the absolute magnitude for each parameter value was taken, and the sum of principal components was normalized to 1. For each model, this process was repeated using 1,000 ensembles containing a random 20% of the full non-oscillatory set. We applied bootstrapping to determine the mean (blue bars) and standard deviation (red lines) of the principal component with the least coefficient of variation. Overall, the enzymatic velocity μ was consistently a sensitive parameter.

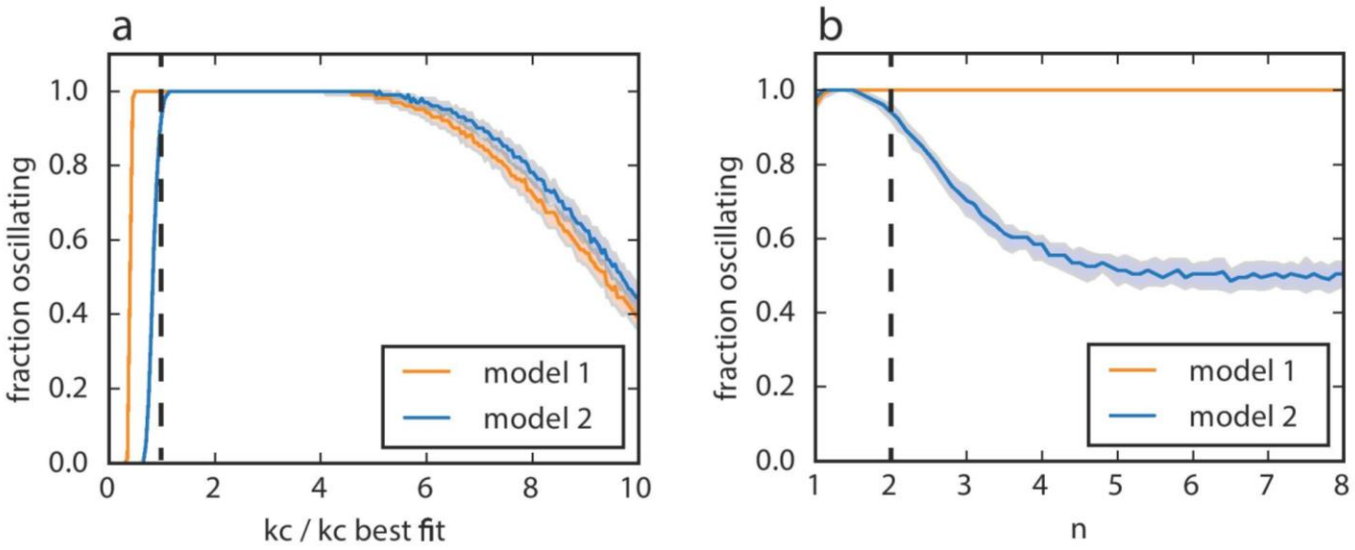

Supplementary Figure 7

The fraction of oscillatory models with a scan of two oscillator parameters.

(a) The cutting rate constant, kc, for I-SceI was varied from 0 to 10-times its best fit value. All other parameters were varied using a uniform distribution ranging ± 5% (similarly as done for Figure 3, e for $\eta = 0.10$, but using 100 ensembles of size 100 each to estimate error). The dashed line indicates the best fit value. (b) We similarly investigated robustness for the cooperativity coefficient n, which was scanned from 1 to 8. The observation that model 2 for both (a) and (b) has fewer nearby parameter sets that oscillate in the vicinity of the best fit is consistent with the picture that model 2 is tuned closer to a bifurcation point.

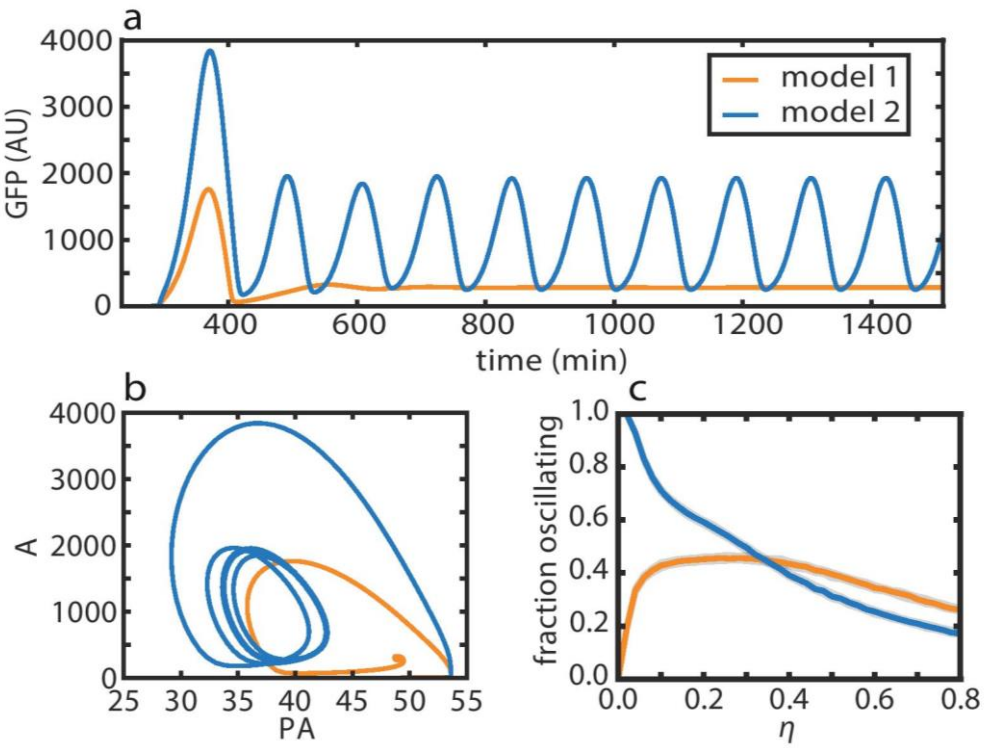

Supplementary Figure 8

Models addressing experimental robustness observations.

To address the observations in Figure 3, where only the circuit with RNAII overexpression feedback oscillated, we examined our model for parameters modified to reflect a change in microfluidic chamber geometry, e.g. leading to slower AHL buildup in the chamber. In particular, we effectively modified the level of LuxI needed to activate the circuit by increasing the parameter value for A0 by 2-fold, and we modified the delay for positive feedback by increasing the parameter value for ktauA by 6-fold. (a) Model 1 did not exhibit oscillations after a short transient, while model 2 exhibited sustained oscillations, as is consistent with experiment. (b) Plasmid copy numbers maintained reasonable values, suggesting plasmid extinction should not be a concern. (c) These solutions were reasonably robust with respect to general parameter variation. Robustness analysis was performed as in Figure 3, e.

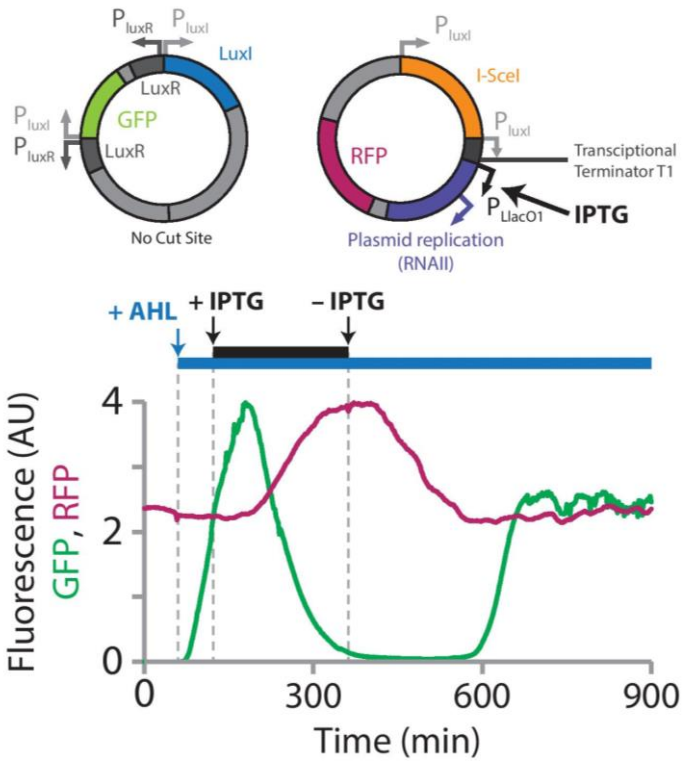

Supplementary Figure 9

Transcription factor titration by plasmid copy number amplification.

p15A copy number amplification counteracts positive feedback from the activator plasmid even without cutting by I-SceI. The activator plasmid used here lacks an I-SceI cut site. The repressor plasmid has been modified to allow inducible plasmid amplification with IPTG, driven by the lac-repressible PLlacO1 promoter. Both *luxI* promoters are left intact, each containing a single LuxR binding site, however the transcriptional terminator downstream of the *luxI* promoters prevents transcription from progressing into the p15A origin. RFP reports on p15A copy number and GFP on *lux* activation state. A small amount of AHL (5 nM) is introduced at t = 1 hour to start *lux* positive feedback from the activator plasmid, causing a rise in GFP signal. At t = 2 hours, 100 μM IPTG is added in addition, causing amplification of the p15A copy number as seen by the rising RFP signal. IPTG is removed again at t = 6 hours, which allows p15A copy number to slowly drop back to natural levels by dilution due to cell division, at which point positive feedback from the activator plasmid resumes.

Table of Strains

Strain	Construct(s) on ColE1 origin plasmid	Construct(s) on p15A origin plasmid	Referenced in Figure
LABS1	Plux-*luxI*-ssrA + *luxR* Plux-*gfp*-ssrA + *luxR* pJ23106-*rfp* (no ssrA)	ParaBAD-*ISceI* (no ssrA)	Fig. 1, a and b Supplementary Fig. 2
LABS2	Plux-*luxI*-ssrA + *luxR* Plux-*gfp*-ssrA + *luxR*	PluxI-*ISceI*-ssrA PJ23106-*rfp* (no ssrA)	Fig. 1, c and d Fig. 2, c: top
LABS3	PluxR-*luxR*	PluxI-*gfp*-ssrA PJ23106-*rfp* (no ssrA) (with copy amplification: PluxI-RNAII)	Fig. 2, a and b Supplementary Fig. 4
LABS4	Plux-*luxI*-ssrA + *luxR* Plux-*gfp*-ssrA + *luxR*	PluxI-*ISceI*-ssrA PJ23106-*rfp* (no ssrA) (with copy amplification: PluxI-RNAII)	Fig. 2, c: bottom, d, and e Fig. 3, a and b
LABS5	Plux-*luxI*-ssrA + *luxR* Plux-*gfp*-ssrA + *luxR* (no I-SceI cut site)	PluxI-*ISceI*-ssrA + 2nd PluxI (terminated) PJ23106-*rfp* (no ssrA) (with IPTG-inducible copy amplification: PLlacO1-RNAII)	Supplementary Fig. 9

Supplementary Table 1. Strains used in this work and gene expression constructs found on each plasmid. All experiments were conducted in *E. coli* MG1655. LABS5 is in strain MG1655-z1, which is modified to express high levels of constitutive lac repressor from the genome. RFP refers to mKate2 and GFP refers to sfGFP. Constructs with promoter ``Plux'' and denoted ``+ *luxR*'' contain the entire bi-directional *lux* promoter (both PluxI and PluxR) and the *luxR* gene. J23106 is a medium-strength constitutive promoter. PLlacO1 is an IPTG-inducuble (i.e. LacI-repressible) promoter. SsrA tags used here code for the amino acids AANDENYALAA and are inserted directly before the stop codon. Plasmid diagrams of LABS1-4 are available in Supplementary Figure 1 and a diagram of LABS5 is available in Supplementary Figure 9.

Nature Genetics: doi:10.1038/ng.3915

Table of qPCR Primers

Primer Set	Forward Primer (5' to 3')	Reverse Primer (5' to 3')
Genomic	GCGAGCGATCCAGAAGATCT	GGGTAAAGGATGCCACAGACA
A	GACGCTCAGTGGAACGAAA	GTAATGACCTCAGAACTCCATCTG
B	CTCGTCAAGAAGGCGATAGAAG	CGTTGGCTACCCGTGATATT
C	CCATTACCTGTCGACACAATCT	GTGTAATCCCAGCAGCAGTTA

Supplementary Table 2. Primers used for determination of relative copy numbers by qPCR. The same genomic reference primers were used in all qPCR experiments. In addition, primer sets A, B, and C were used for measuring copy number repression using strain LABS1, while primer set C was used for measuring copy number amplification using strain LABS3.

Supplementary Note: Synchronized DNA cycling across a bacterial population

1 Details of the Quantitative Model

We explored a number of models for the experimental oscillators. The simplest models considered the dynamics for the concentrations of LuxI, I-SceI, GFP, and the plasmid expressing LuxI, with the constraint that the concentrations of GFP and I-SceI are simply proportional to LuxI. These two-dimensional models with appropriate parameter values produced oscillations reminiscent of experimental trajectories (results not shown), which demonstrates that the basic elements of gene regulation-based positive feedback coupled to plasmid copy number regulation-based negative feedback are theoretically sufficient for oscillations.

These suggestive results prompted us to explore a more complex *empirical* model with additional elements, leading to a model that includes gene regulation-based positive feedback, plasmid copy number regulation-based negative feedback, intracellular delay in feedback, and proteolytic queueing effects, all of which are known to potentially be important based on the design of the circuit and based on prior studies. These additional details led to a model that can both describe aspects of the experimental data and also be relatively robust with respect to parameter variation, as Supplementary Note Section 3 will discuss. It is worth noting that we found a few qualitatively similar parameter sets for the model that all fit experimental data comparably, so we picked our final parameter set based largely on robustness.

Nature Genetics: doi:10.1038/ng.3915

The model considers the dynamics of five key variables: the concentrations of LuxI (labeled A), I-SceI (labeled S), GFP (labeled G), the plasmid expressing LuxI (labeled PA), and the plasmid expressing I-SceI (labeled PS). Concentrations are indicated by square brackets, e.g. the concentration $[\mathrm{A}]$ for species A. Furthermore, we include explicit dynamics for $\mathrm{A_i}$, $\mathrm{S_i}$, $\mathrm{PA_i}$, and $\mathrm{PS_i}$ ($i = 1, 2, ...5$), which effectively model a delay in the production of species or perhaps a delay in the feedback on the species. These effective intermediate species were introduced, because we expect delay to exist for both protein production and plasmid production in the experimental context. Note that we use the concentration $[\mathrm{A}]$ as an effective proxy for the concentration (up to some scale) of other activating species, such as AHL, to simplify our system.

These species are governed by the following reactions, where the reaction velocities are assumed to have appropriate mass action terms included. Production of precursors for activator and repressor follow from the respective reactions

$$\mathrm{PA} \xrightarrow{F([\mathrm{A}])} \mathrm{PA} + \mathrm{A_1} \tag{1}$$

$$\mathrm{PS} \xrightarrow{F([\mathrm{A}])} \mathrm{PS} + \mathrm{S_1} \tag{2}$$

Note that the velocity of these reactions depends linearly on plasmid concentrations due to mass action terms, which allows plasmid copy number to influence gene expression. $F([A])$ encodes gene regulation by the act of LuxI producing AHL, which in turn activates p_{LuxI} promoters. $F([A])$ can be written

$$F([\mathrm{A}]) = \frac{\alpha \cdot \left(1 + f \cdot \left(\frac{[\mathrm{A}]+H0}{A0}\right)^n\right)}{1 + \left(\frac{[\mathrm{A}]+H0}{A0}\right)^n} \tag{3}$$

Nature Genetics: doi:10.1038/ng.3915

where α is the maximum production rate (per plasmid), f characterizes the strength of gene activation by A (value constrained by $f \geq 1$), n is the cooperativity of gene activation (set to $n = 2$, but allowed to vary in our robustness analysis), $A0$ is the value of [A] required to strongly activate gene expression, and $H0$ allows for a generally time-dependent background level of AHL that can stimulate activation. We assume that the background level of $H0$ increases suddenly from $a0$ to $a1$ at a time t_0, obeying the equation

$$H0 = a0 \cdot (1 - \theta(t - t_0)) + a1 \cdot \theta(t - t_0) \tag{4}$$

with θ the Heaviside step function.

Production of the intermediates, A_1 and S_1, eventually leads to the arrival of mature forms A and S, respectively, via the reactions

$$\mathrm{A_i} \xrightarrow{ktauA} \mathrm{A_{i+1}}\ , \quad i = 1,2,..,4 \tag{5}$$

$$\mathrm{A_5} \xrightarrow{ktauA} \mathrm{A} \tag{6}$$

$$\mathrm{S_i} \xrightarrow{ktauS} \mathrm{S_{i+1}}\ , \quad i = 1,2,..,4 \tag{7}$$

$$\mathrm{S_5} \xrightarrow{ktauS} \mathrm{S} \tag{8}$$

with *ktauA* and *ktauS* being rate constants that characterize the delay in production (effectively a feedback delay), with respective associated mean delay $5/ktauA$ and $5/ktauS$. These delays appeared to be important to fit the initial large pulse of GFP seen in experiment.

The proteins *A* and *S* are tagged for rapid degradation by the protease ClpXP, so we model

their degradation using enzymatic kinetics. This is modeled by the reactions

$$\mathrm{A} \xrightarrow{GA([\mathrm{A}],[\mathrm{S}])} \varnothing \tag{9}$$

$$\mathrm{S} \xrightarrow{GS([\mathrm{A}],[\mathrm{S}])} \varnothing \tag{10}$$

with functions

$$GA([\mathrm{A}],[\mathrm{S}]) = \frac{\mu \nu_1}{K + \nu_1[\mathrm{A}] + \nu_2[\mathrm{S}]} \tag{11}$$

$$GS([\mathrm{A}],[\mathrm{S}]) = \frac{\mu \nu_2}{K + \nu_1[\mathrm{A}] + \nu_2[\mathrm{S}]} \tag{12}$$

where μ is the maximum degradation velocity, and the parameters K, ν_1, and ν_2 characterize the affinities of protein to the protease. Recall that mass action terms should be included in the reaction velocities.

Cutting of PA is modeled by a bimolecular reaction that allows S to degrade PA

$$\mathrm{PA} + \mathrm{S} \xrightarrow{kc} \mathrm{S} \tag{13}$$

with *kc* the cutting rate constant. We assume then that the act of cutting immediately degrades the activator plasmid, which is likely reasonable given that we expect linearized DNA to be degraded within the cell. It is possible that linearized DNA could re-circularize, but we do not model this. It is also possible that re-circularization may only effectively modify (reduce) the rate constant *kc*.

Proteins are assumed to be diluted due to cell growth and division. This is modeled by the

reactions

$$\mathrm{A} \xrightarrow{ga} \varnothing \tag{14}$$

$$\mathrm{S} \xrightarrow{gs} \varnothing \tag{15}$$

with $ga = gs = \ln 2/30.0$ min. the dilution rate. Plasmids are assumed to be degraded also by dilution, so we set

$$\mathrm{PA} \xrightarrow{k} \varnothing \tag{16}$$

$$\mathrm{PS} \xrightarrow{k} \varnothing \tag{17}$$

with $k = \ln 2/30.0$ min. We will allow ga, gs, and k to be varied independently in our robustness analysis, even though we set them to have the same value here.

For the oscillator without the effect of read-through on the repressor plasmid (termed Model 1), we model plasmid production by the production of an intermediate, e.g. PA_1 representing a partially replicated plasmid. Production follows from the reactions

$$\varnothing \xrightarrow{k \cdot PA0} \mathrm{PA}_1 \tag{18}$$

$$\varnothing \xrightarrow{k \cdot PS0} \mathrm{PS}_1 \tag{19}$$

where the parameters $PA0$ and $PS0$ allow different plasmid copy numbers for activator and repressor plasmids. Plasmid intermediates eventually lead to an complete plasmid by the additional

reactions

$$\mathrm{PA_i} \xrightarrow{ktauPA} \mathrm{PA_{i+1}}\ ,\ \ i = 1,2,..,4 \tag{20}$$

$$\mathrm{PA_5} \xrightarrow{ktauPA} \mathrm{PA} \tag{21}$$

$$\mathrm{PS_i} \xrightarrow{ktauPS} \mathrm{PS_{i+1}}\ ,\ \ i = 1,2,..,4 \tag{22}$$

$$\mathrm{PS_5} \xrightarrow{ktauPS} \mathrm{PS} \tag{23}$$

which are analogous to the corresponding reactions for A and S. Notice that we do not allow plasmid extinction using this scheme, but we will check self-consistently that plasmid copy numbers do not become so low that extinction is likely to be an issue.

For the oscillator with the effect of read-through affecting repressor plasmid copy number (Model 2), we replaced the production reaction for $\mathrm{PS_1}$ by the reaction

$$\varnothing \xrightarrow{R([\mathrm{A}])} \mathrm{PS_1} \tag{24}$$

with

$$R([\mathrm{A}]) = k \cdot PS0 \cdot \frac{fPS1 + fPS2 \cdot \left(\frac{[\mathrm{A}]}{APS}\right)^{nPS}}{1 + \left(\frac{[\mathrm{A}]}{APS}\right)^{nPS}} \tag{25}$$

with parameters $fPS1$, $fPS2$, APS, and nPS parameters characterizing this function. We set $fPS1 = 1$ and $nPS = 1$, but we allow these parameters to vary in our robustness analysis. Note that again, we use $[A]$ as a proxy for the concentration (to to some scale) of other activator species.

The concentration of GFP ([G]) is assumed to always be proportional to [A], though the proportionality constant is allowed to vary slightly from experiment to experiment to account for

variations in lamp intensity, etc. Thus, GFP effectively does not play any important dynamical role in the model.

Finally, all concentrations are divided by a fictitious standard volume, $V0$. We normalize this volume to $V0 = 1$, though this parameter is allowed to vary in our robustness analysis.

2 Fitting the Model Using COPASI

We encoded our model into the simulation package COPASI for basic simulation and fitting. COPASI provides several advantages: an environment that is readily installed on a variety of platforms, an ability to import from and export to a variety of model formats, and inclusion of numerous tasks (including model fitting) that can be run on models.

The numerous unknown parameters in the model prompted us to attempt automated fitting of the time-course data to determine these parameters. Within COPASI, we fitted the model to experimental data by (1) importing two representative experimental mean GFP trajectories (averaging across a whole microfluidic chamber) for the circuits without and with read-through feedback, (2) configuring COPASI's Parameter Estimation task to simultaneously fit these two experimental results to our model, (3) ensuring the model has run to near steady state before experimental data is compared to the model (by allowing the first pulse of the experimental oscillator to be occur at a late time, roughly at 300 min.), and (4) running the Parameter Estimation task with given constraints on parameter sizes and with a given fitting method. We used deterministic integration to simulate the model when comparing it to experimental data, using the LSODA method with

Nature Genetics: doi:10.1038/ng.3915

relative tolerance 10^{-6} and absolute tolerance 10^{-12}. Fitted parameters followed by attempting to minimize the root-mean-square error between the model's trajectory for GFP concentration and the measured mean GFP in experiment. Recall that we assume GFP concentration is proportional to [A].

The above step (4) was executed many times to find a model that optimized accuracy. First, global optimization techniques, such as the COPASI method "Evolutionary Strategy," were used to find broad regions of parameter space with accurate solutions. These methods were followed with local optimization methods in COPASI, such as "Hooke and Jeeves," to further increase accuracy. We ultimately found a deterministic ODE model that was both accurate and exhibited reasonable robustness, the latter of which is discussed in the next section. We use the term "Model 1" for the model where read-through does not affect repressor plasmid copy number, while we use the term "Model 2" for the model where read-through does affect repressor plasmid copy number. These models share the same parameters, except that Model 2 has additional parameters to characterize the potential effects of read-through.

Our final parameter set for our model fit is reported in Supplementary Note Table 1.

3 Robustness Analysis of the Quantitative Model

We checked whether our model was robust, i.e. it produces oscillations for a wide range of parameter values. For models with few (~ 2) parameters, robustness can be checked using bifurcation diagrams. However, our model has many parameters, and a standard bifurcation analysis may not

properly reflect any underlying robustness. To address these concerns, we performed a robustness analysis that samples many parameter sets around our fitted parameter set, and we tested whether these parameter sets corresponded to oscillations. Custom Python software was written to translate C-code output from COPASI into fast Python code, since COPASI was apparently unable to perform the robustness analysis we desired. The scipy.integrate.odeint module in the scipy library was used, with relative tolerance 10^{-6} and absolute tolerance 10^{-12}.

Robustness was explored as follows. We scanned a parameter η from 0.00 to 0.80 in increments of 0.02. For each value of η, we constructed 100 parameter ensembles that each consisted of 1000 random parameter sets. A random parameter set is generated by multiplying the respective fitted value of every parameter in Supplementary Note Table 1 by an independent random number uniformly distributed between $1-(\eta/2)$ and $1+(\eta/2)$. This samples a large hypervolume of parameter space that is difficult to obtain using bifurcation diagrams. A trajectory was determined to be oscillatory if the standard deviation (across time) of the trajectory $[\mathrm{A}](t)$ exceeded 10% of the mean (across time) during a specific window of time. For simulations starting at time $t = 0$, this window of time was 814-1512 min. for Model 1 (without read-through effects) and 862-1510 min. for Model 2 (with read-through effects). The time each model was induced was $t_0 = 288$ min.

Figure 3, e reports the robustness based on this analysis. These statistics support that Model 1 is generally more robust than Model 2 with respect to oscillations. We suspect this is due to Model 2 being tuned closer to a bifurcation such as a Hopf bifurcation, which would lead to GFP oscillations that appear more sinusoidal in shape, i.e. not relaxing to zero during each oscillation.

Nature Genetics: doi:10.1038/ng.3915

The trajectories of mean GFP for the experimental construct with read-through regulation exhibit similar oscillations as in Model 2, i.e. oscillations that do not relax to zero (background) intensity. Thus, our numerical results and this overall logic suggest that the experimental construct with read-through regulation should be less robust.

We quantified the most sensitive parameters with respect to robustness using the same data set as above (the scan of η). For each ensemble of 1000 trajectories, we construct a non-oscillatory set consisting only of parameters not leading to oscillations (by our above test). Within this non-oscillatory set, the principal component with the lowest coefficient of variation (standard deviation divided by the mean) was determined. The idea is that the most sensitive parameters would have a narrow distribution in the non-oscillatory set, since a parameter that does not heavily influence the stability of oscillations would have a wide distribution (sampling most of the default fractional range $1-(\eta/2)$ and $1+(\eta/2)$). We report out results from this principal component analysis in Supplementary Figure 6. We found that the degradation velocity μ was a key sensitive parameter in this investigation, which is not terribly surprising given the important role of degradation in oscillatory dynamics.

Nature Genetics: doi:10.1038/ng.3915

Name	Description	Value	Name	Description	Value
A0	parameter for the production rate of LuxI and I-SceI	1105.9400	gs	dilution rate of I-SceI	0.0231
APS	parameter for RNAII overexpression copy number control	929.4370	k	dilution rate of plasmid	0.0231
K	parameter for enzymatic degradation	100.7700	kc	I-SceI cutting rate constant	4.8375×10^{-5}
PA0	scale of activator plasmid copy number	53.7116	ktauA	effective delay rate constant for LuxI production	0.1810
PS0	scale of repressor plasmid copy number	11.3784	ktauPA	effective delay rate constant for activator plasmid production	0.2141
V0	volume of cell in natural units	1.0	ktauPS	effective delay rate constant for repressor plasmid production	0.1155
a0	the background level of AHL before induction (AU)	0.0	ktauS	effective delay rate constant for I-SceI production	0.3536
a1	the background level of AHL after induction (AU)	2296.6800	μ	enzymatic degradation velocity of proteins	698.8910
α	maximum production rate per plasmid for LuxI and I-SceI	0.6582	n	cooperativity parameter for LuxI and I-SceI production	2
f	fold activation for saturating AHL vs. absent AHL in for LuxI and I-SceI production	27.7632	nPS	cooperativity parameter for RNAII overexpression copy number control	1
fPS1	parameter for RNAII feedback	1.0	v_1	parameter for enzymatic degradation	3.4699
fPS2	parameter for RNAII feedback	3.4870	v_2	parameter for enzymatic degradation	4.9963
ga	dilution rate of LuxI	0.0231			

Supplementary Note Table 1: Parameter names and corresponding values for our optimized model fit. Time is in units of minutes. Concentrations and other physical units are dimensionless (AU).